Observation of banded spherulite in a pure compound by rhythmic growth

Subhadip Ghosh, Dipak Patra, and Arun Roy*
Soft Condensed Matter Group, Raman Research Institute, Bangalore 560080, India

(Received 27 January 2022; revised 22 March 2022; accepted 20 April 2022; published 3 May 2022)

Banded spherulitic growth of crystals is observed in some materials with spherically symmetric growth front and periodic radial variation of birefringence. This variation of birefringence in quasi-two-dimensional geometry produces concentric interference color bands when viewed through crossed polarizers. In most materials, the banded spherulites are found to be formed by radially oriented periodically twisted fibrillar crystallites. Here, we report the formation of banded spherulites due to the rhythmic growth of concentric crystallite-rich and crystallite-poor bands for a pure compound consisting of strongly polar rodlike molecules. The compound exhibits coexistence of untwisted fibrillar crystallites and an amorphous phase in its most stable solid state. On sufficient supercooling of the sample from its melting point, the banded spherulites are formed with a periodic variation of composition of untwisted radially aligned fibrillar crystallites and an amorphous solid phase. We have developed a time-dependent Ginzburg-Landau model to account for the observed banded spherulitic growth.

DOI: 10.1103/PhysRevMaterials.6.053401

I. INTRODUCTION

The spherulitic growth of solids is a ubiquitous phenomenon exhibited by many different types of materials such as polymers [1,2], minerals [3–5], elements [6,7], metals [8], and salts [9–11]. It is also found in biological materials like coral skeletons [12], kidney stones [13], proteins [14–16], and urinary sediments [17]. In spherulitic growth, the solid phase after nucleation grows with a spherical growth front with continuous orientational symmetry in contrast to the growth of a crystal having discrete orientational symmetries. The spherulites were initially named as "circular crystals" for its circular boundary in quasi-two-dimensional geometry which changed later to spherulite [18]. In spite of research on it for over a century, the detailed understanding of the mechanism of this abundantly found natural growth phenomenon is still incomplete [8]. The spherulitic growth morphology is often associated with the formation of many radially aligned fibrillar crystallites which branch noncrystallographically for filling space during the growth [19]. This distinct characteristic of spherulites separates them from the other polycrystalline aggregates.

For some materials, the spherulitic growth is accompanied by a series of equidistant concentric bands and is known as banded spherulite. In quasi-two-dimensional geometry, the banded spherulite domain appears as a flattened disk with circular boundary and these bands appear as concentric circular rings. The polarizing optical microscopic textures of these spherulites show concentric bands with periodic variation of interference color. Polymers generally form this kind of banded spherulite [1,2,8,20]. Some small molecular systems also produce banded spherulites [21–28]. An organized periodic twisting of radially aligned fibrillar crystallites in the banded spherulitic domain has been observed to generate a periodic change of effective birefringence along the radial direction. This undulation in the birefringence gives rise to concentric bands with periodic variation of colors when viewed through crossed polarizers. In contrast, some multicomponent blends of materials form banded spherulites by rhythmic deposition of host and additive materials [29–31]. Even in some of these cases, twist order of fibrils has been found to contribute to the modulation of effective birefringence along the radial direction. So the organized twisting of the fibrillar crystallites is considered to be a primary mechanism for the formation of the banded spherulites.

Besides banded spherulite, the rhythmic growth of ring banded structures formed on thin films with one free surface has been reported [32–40]. The periodic height modulation of the free surface gives rise to the ring banded structure in these systems. The effective birefringence in these cases may also vary periodically depending on the periodic orientational change of lamellar building blocks. The diffusion controlled growth mechanism produces a rhythmic variation of material supply near the growth front of the solid phase which leads to this height modulation. These types of ring banded structures are found only in thin films and are very different from the banded spherulites formed in three-dimensional bulk systems [2].

In this work, we report the formation of banded spherulite by a pure liquid crystalline compound consisting of relatively small rodlike molecules. We show that the rhythmic growth of concentric crystallite-rich and crystallite-poor zones is the underlying mechanism for the formation of banded spherulites of this compound contrary to the organized twisting of the fibrillar crystallites. The crystallite-rich zones have higher density of radially aligned fibrillar nanocrystallites while crystallite-poor zones are rich in the solid amorphous state

*aroy@rri.res.in

of the compound. The alternation of these concentric regions changes the effective birefringence periodically along the radial direction of the spherulite giving rise to the concentric interference color bands between crossed polarizers. We also develop a phase field model to account for the formation of banded spherulite due to rhythmic growth in our system.

II. EXPERIMENT

The commercially available liquid crystalline compound 4′-octyloxy-4-cyanobiphenyl (8OCB) was used with 99% purity. For spherulitic growth, the sample sandwiched between two cleaned cover slips in its isotropic phase was cooled to a desired temperature (T) below its melting point (T_m) using a microscope hot stage (Linkam). The banded spherulitic domains of the sample were generally formed above the supercooling $\Delta T = (T_m - T) = 22.5$ K. The spherulitic domains grown in this way were used for polarizing optical microscope (POM) observations and Raman spectroscopic studies. The spacing between the spherulitic bands was determined by taking photographs using a digital camera (Canon EOS 80D) attached to the polarizing microscope (Olympus BX50) followed by analysis of the images using the imageJ software.

The micro-Raman spectroscopic studies of the spherulite domain were performed using a Raman spectrometer (Jabin-Yvon T64000) equipped with a nanopositioning stage. An air-cooled argon laser (Melles Griot) beam of wavelength 514 nm was used as an excitation source. An objective lens with 50× magnification and 0.75 numerical aperture was used to focus the beam on the sample. The Raman spectra of the sample were recorded from the backscattered light. The theoretically estimated diameter of the focused spot is less than 1 μm.

The field emission scanning electron microscopy (FESEM) studies of the spherulite domain were conducted using the CARL ZEISS (ULTRA PLUS model) system. The banded spherulites of the sample were formed from its melt on cleaned ITO-coated glass plates at room temperature. The free surface of these samples was sputter coated with platinum [QUORUM (Q150R S)] for FESEM imaging. For the cross-sectional view of the domain, the spherulites formed on cover slips were cleaved in the middle and then the cross-sectional areas were sputter coated with platinum for FESEM imaging.

The fluorescent dye (rhodamine 6G) was mixed with the 8OCB sample at $1{:}10^4$ wt/wt ratio. The mixture was stirred for 3 hours above the clearing temperature of 8OCB for homogeneous mixing. The sample was then sandwiched between two cover slips and supercooled to room temperature to form the banded spherulites. The fluorescent images of the spherulite domain were captured by a confocal microscope (Leica SP8) equipped with an argon gas laser. The exciting wavelength was 514 nm.

A DY 1042-Empyrean (PANalytical) x-ray diffractometer with a PIXcel 3D detector was used to acquire the x-ray diffraction (XRD) profiles of the sample using Cu $K\alpha$ radiation of wavelength 1.54 Å. The banded spherulites were formed on a cleaned cover slip on cooling the sample to room temperature from its isotropic phase and its formation was confirmed by POM observation. The sample was then scraped off this substrate and placed on a silicon plate. The XRD measurements were performed in the grazing angle of incidence of the x-ray beam. The silicon plate has a flat XRD profile which does not interfere with that from the sample.

The temperature variation of the dielectric constant of the sample was measured using a homemade setup. The detail of this setup has been discussed elsewhere [41]. A commercially available liquid crystal cell (INSTEC Inc.) of sample thickness 5 μm and electrode area 5×5 mm^2 was used for dielectric measurement. Prior to filling the sample, the capacitance of the empty cell was measured. The cell was then filled with the sample in its isotropic phase by capillary action on a hot stage. After that, it was supercooled to the lower temperature to form banded spherulite domains. The formation of the banded spherulites was confirmed using POM observation of the sample. A sinusoidal voltage of rms amplitude 0.5 V and frequency 5641 Hz was used for the dielectric measurements. The ratio of the capacitance of the filled cell to the empty cell gives the dielectric constant of the sample.

III. RESULTS AND DISCUSSION

The liquid crystalline compound 4′-octyloxy-4-cyanobiphenyl abbreviated as 8OCB exhibits a variety of crystal and liquid crystal phases. The sample shows a melting transition to the smectic-A phase at 327.6 K on heating from its most stable crystal phase known as the commercial powder or CP phase. On further heating, the compound transforms to the nematic and to the isotropic liquid phase at 340.1 K and 353.1 K, respectively. The sample exhibits a large range of supercooling from its smectic-A phase. The banded spherulitic domains are formed on supercooling the smectic phase by at least 22.5 K below the melting temperature. The probability of getting the banded spherulites increases with higher supercooling.

These banded spherulites generally show four black brushes parallel to the polarizers forming a Maltese cross in addition to the concentric interference color bands between crossed polarizers. These color bands arise from the periodic variation of the effective birefringence in the sample along the radial direction. Figure 1(a) shows a polarizing optical microscope (POM) texture of a banded spherulite formed between two cover slips on cooling the sample to room temperature. The black and white appearance of the interference color bands in this texture is due to relatively lower thickness of the sample with phase retardation in the first-order region of the Levy chart. The dark arms of the Maltese cross remain invariant on rotating the sample between crossed polarizers. This implies that the major axis of the effective refractive index ellipse in the plane perpendicular to the light path lies parallel or perpendicular to the radial direction of the spherulitic domain.

The POM studies using a λ plate (530 nm) were performed to determine the orientation of this major axis. Figure 1(b) is the POM image after introducing the λ plate in the optical path of the microscope. The yellow double-headed arrow shows the orientation of the slow axis of the λ plate with respect to the orientations of the crossed polarizers. It can be inferred from the Levy chart that there is effective addition and subtraction of path differences due to the sample and the λ plate in the blue and yellow colored regions of the texture, respectively. This observation clearly indicates that the major axis is oriented

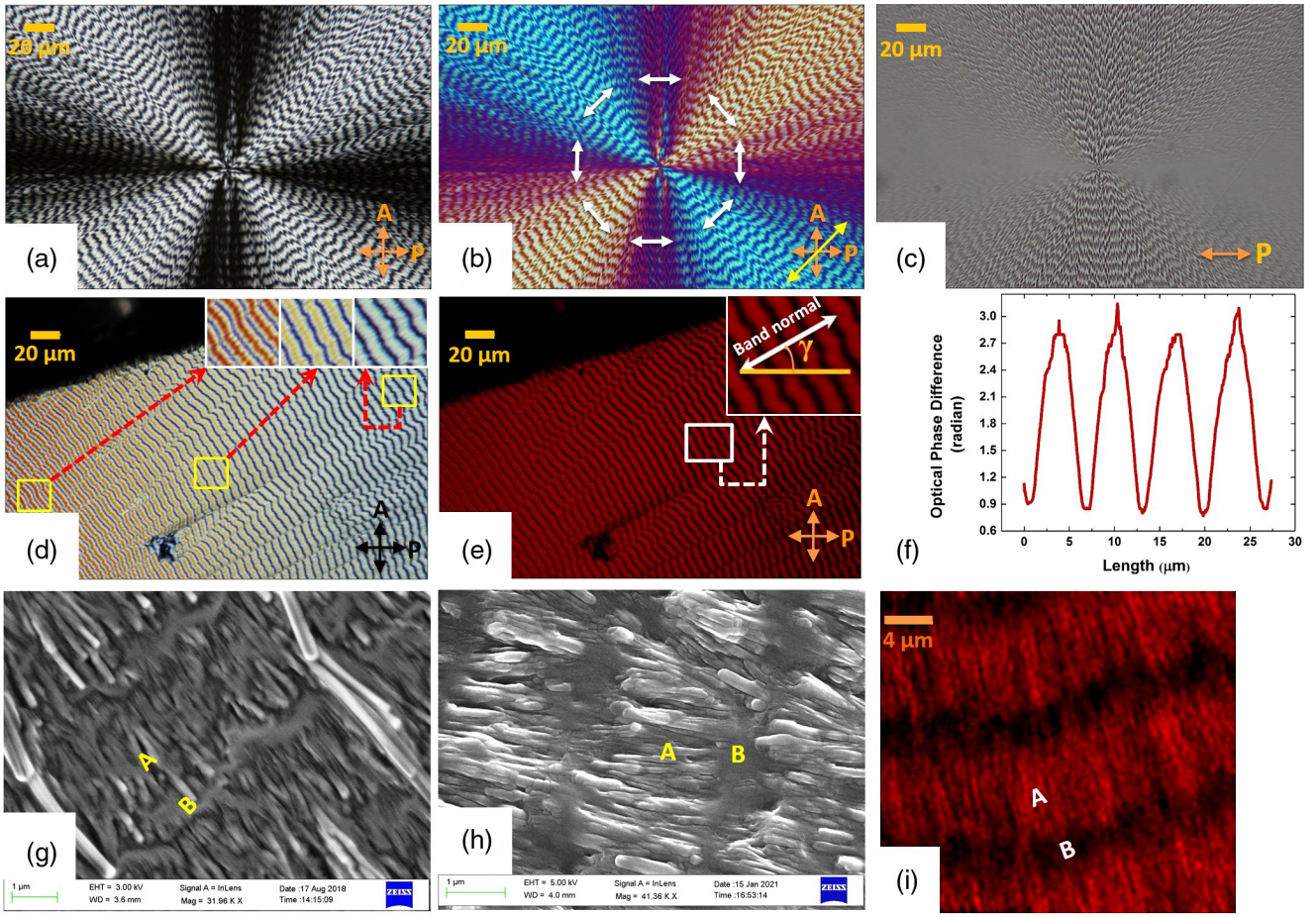

FIG. 1. Microscopic textures of banded spherulite. The POM textures of banded spherulite of compound 8OCB at room temperature (a) between crossed polarizers, (b) between crossed polarizers and a λ plate, and (c) with only the polarizer in the optical path. The white double-headed arrows in (b) indicate the orientations of major refractive index around the seed. (d) The POM texture of a banded spherulite domain between crossed polarizers for relatively thicker sample at room temperature. The insets show the variation of color in the bands in three different regions with slightly different sample thickness. (e) The same as in (d) with a red filter introduced in the optical path. The inset shows the variation of light intensity along the band normal which makes an angle γ with the polarizer. (f) The variation of optical phase difference along the radial direction of the banded spherulite shown in (e). The FESEM image of (g) the top surface of a banded spherulite and (h) the cross-sectional view of a banded spherulitic obtained from the cleaved surface showing the bulk structure. (i) The fluorescent image of a dye-doped banded spherulite at room temperature. The regions marked "A" and "B" represent the concentric crystallite-rich and crystallite-poor bands, respectively.

parallel to the azimuthal direction of the banded spherulite. Hence the spherulite observed for this sample is optically negative [1,8]. The white double-headed arrows in Fig. 1(b) show the orientation of the major axis around the seed of this spherulite domain. The spacing between successive bands is also measured for different values of supercooling of the sample and compared with the theoretical results discussed later. The band spacing does not vary appreciably with the thickness of the sample (see Fig. S1 in the Supplemental Material [56]) which also agrees with our theoretical model.

Figure 1(c) is the bright-field image of the sample shown in Fig. 1(a) with only the polarizer in the light path. In this figure, the bands have low (high) optical contrast where band normal is parallel (perpendicular) to the polarizer. These observations indicate that the radial component of refractive index does not vary appreciably along the radial direction but the strong variation of the azimuthal component along the radial direction produces the undulation of the birefringence in the spherulite.

For relatively thicker sample, there are multiple interference color rings in a given spherulitic band as shown in Fig. 1(d). The insets in Fig. 1(d) are the magnified view of these interference color rings in three regions with slightly different sample thickness. The variation of phase retardation in the texture can be measured from the intensity variation by introducing a red filter in the light path of the POM. Figure 1(e) is the POM image of the spherulite domain with a periodic variation of intensity along the radial direction of the spherulite. The inset in Fig. 1(e) depicts the magnified view of the marked region of this domain where the band normal makes an angle $\gamma = 30.5^\circ$ with respect to the polarizer. Then the phase retardation can be calculated from the formula $I = I_0 \sin^2(2\gamma) \sin^2(\phi/2) + I_d$, where I_0, I, and I_d are the incident, measured, and the dark background intensities with crossed polarizers, respectively. The phase retardation $\phi = 2\pi d \Delta n/\lambda$, where d is the sample thickness, Δn is the effective linear birefringence of the sample, and λ is the

wavelength of incident light. Figure 1(f) shows the measured variation of optical phase retardation along the radial direction of the spherulite. The variation of sample thickness for the selected small region shown in the inset of Fig. 1(e) is negligible and the oscillation of phase retardation across the bands mainly arises due to the variation of the birefringence in the sample.

The field emission scanning electron microscopy (FESEM) studies of the banded spherulite domain showed concentric bands with same periodicity as found in POM studies. The high-resolution FESEM texture of the spherulitic domain revealed that it consists of numerous fibrillar nanocrystallites embedded in an amorphous phase. The bands in the spherulite arise from the periodic growth of crystallite-rich and crystallite-poor concentric zones as shown in Fig. 1(g). Similar repetitive structure was also found in the FESEM texture of the bisected cross-sectional surface area of the sample [Fig. 1(h)] showing its bulk nature (also see Fig. S2 in the Supplemental Material [56]). The FESEM textures of the sample revealed that the crystallite-rich zones (marked as "A") have high density of fibrillar crystallites aligned along the radial direction while crystallite-poor zones (marked as "B") are rich in solid amorphous state of the compound. The crystallites have length similar to the periodicity of the bands while the width varies from 100 nm to 300 nm.

Some polymers and a few small molecular systems exhibit concentric color banded spherulites [1,2,8,20–25] in which organized twisting of fibrillar units along their long axis has been observed as the mechanism of the band formation. In some small molecular systems, a periodic variation of orientation of individual crystallites has been reported to produce concentric color bands [42,43]. But in our sample, neither twist nor periodic change of orientation of fibrillar crystallites is found. The FESEM studies depict that the rhythmic growth of concentric crystallite-rich and crystallite-poor zones produces the banded spherulite of 8OCB. The periodic change in birefringence along the radial direction due to these concentric zones gives rise to the interference color bands observed between crossed polarizers. The crystallite-poor regions possess least birefringence due to their predominant amorphous nature while the crystallite-rich zones have larger birefringence due to the presence of a large number of radially aligned crystallites.

A fluorescent image of the banded spherulite domain [see Fig. 1(i)] was obtained by doping the sample with a fluorescent dye (rhodamine 6G). It shows a periodic variation of dye concentration along the radial direction of the spherulite domain. The crystallite-rich zones are found to have higher concentration of dye molecules compared to the crystallite-poor zones which makes these zones brighter and darker, respectively, in the fluorescent image. The dynamic advection of the dye molecules during the growth of crystallite-rich and crystallite-poor zones perhaps can explain their distribution in the banded spherulite of the sample. The molecular density is higher in crystallite-rich zones compared to crystallite-poor regions. Thus the growth of a crystallite-rich band produces a diffusive current which advects the dye molecules from the leading edge of the growth front that gives rise to the higher density of the dye molecules in this band. The depletion of molecular density promotes the formation of crystallite-poor zones with lower density of the dye molecules. The repetition of these processes leads to the formation of banded spherulite in this sample.

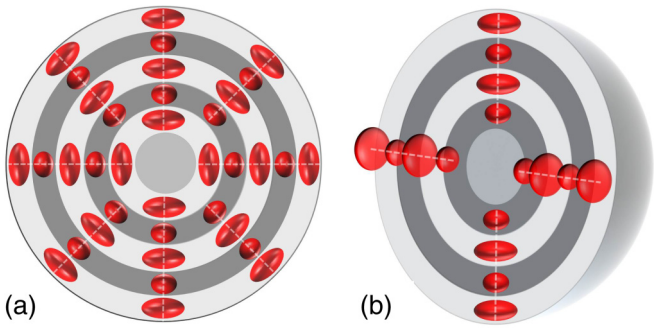

FIG. 2. Indicatrix ellipsoid in banded spherulite. The schematic representation of the variation of optical indicatrix along the radial direction of the banded spherulite of the compound 8OCB. The (a) top and (b) side views showing the uniaxial oblate indicatrix with radially oriented optic axes.

Figure 2 shows the schematic representation of the variation in the refractive index ellipsoid along the radial direction of the banded spherulite. The FESEM studies revealed that the elliptical or rectangular cross sections of radially aligned fibrillar crystallites are oriented randomly in the banded spherulite giving rise to a uniaxial structure about the radial direction (see Fig. S3 in the Supplemental Material [56]). The POM studies showed that the azimuthal component of the refractive index is larger than the radial component in the spherulite. Hence, the banded spherulite of 8OCB possesses a uniaxial oblate indicatrix with a radially oriented optic axis as shown in Fig. 2. The radial component of the refractive index does not vary appreciably along the radial direction but the periodic variation of the transverse component gives rise to the modulation in the birefringence of the sample as observed in Fig. 1(c).

The x-ray diffraction (XRD) studies were performed to identify the crystal structure of the banded spherulite domain. The XRD profile [Fig. 3(a)] of the banded spherulite is identical to that of the commercial powder or CP crystal phase of 8OCB. We have recently shown that the CP crystal phase is composed of fibrillar nanocrystallites of the compound embedded in its own amorphous solid state [41]. All the peaks observed in the XRD profile are associated with the monoclinic crystal structure of the nanocrystallites. The amorphous component shows only a broad hump from 11 nm^{-1} to 21 nm^{-1} in this XRD profile. Thus the XRD studies indicate that the banded spherulite of the compound has similar composition as its CP crystal phase.

The spatially resolved variation in the compositions of the sample in the banded spherulitic domain was probed by micro-Raman spectroscopy. The stretching vibration peak at 2235 cm^{-1} of the nitrile (CN) bond of 8OCB molecules was used to examine the compositions of the spherulite along its band normal direction. This Raman peak is reported to be quite sensitive to the molecular environment around the CN bond of this molecule [44]. It is asymmetric in the spherulite domain and can be fitted with two closely spaced peaks (see Fig. S4 in the Supplemental Material [56]). The fitted intense

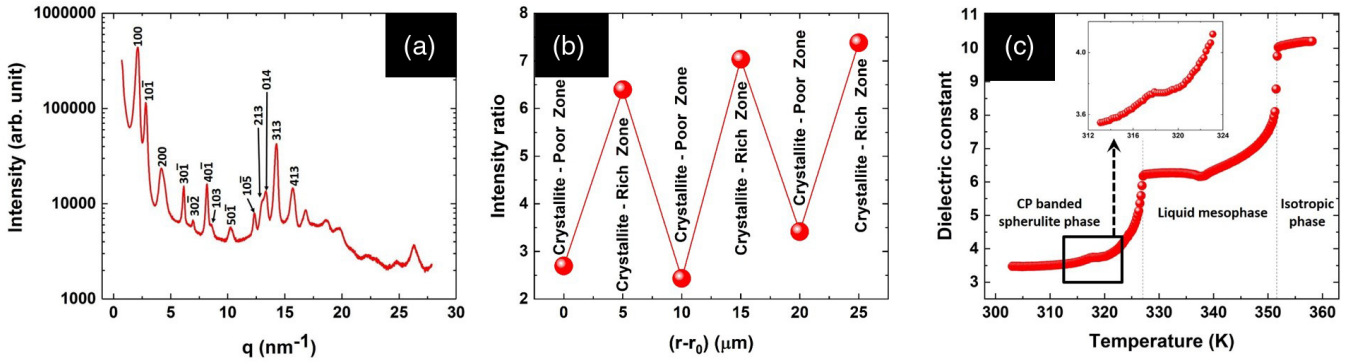

FIG. 3. Two phase coexistence from XRD, Raman, and dielectric profile. (a) The XRD profile of the banded spherulite of the compound 8OCB. (b) The variation of intensity ratio of the Raman peaks associated with the CN group of the molecules at few consecutive crystallite-rich and crystallite-poor bands along radial direction of the banded spherulite where r_0 is an initial point of measurement. (c) The variation of dielectric constant of the banded spherulite with temperature during heating of the sample. The inset highlights the step change in dielectric constant at 318.1 K.

peak positioned at 2235 cm^{-1} arises from the nanocrystallites of the banded spherulite and the less intense shoulder peak positioned at 2226 cm^{-1} originates from the amorphous component [41]. The ratio of the intensities of these peaks obtained in the crystallite-rich and crystallite-poor zones along the radial direction of the banded spherulite is shown in Fig. 3(b). The higher and lower values of this intensity ratio at crystallite-rich and crystal-poor zones, respectively, indicate the periodic variation of the compositions along the radial direction of the banded spherulite.

The temperature variation of dielectric constant of the banded spherulite sample during heating it from room temperature is shown in Fig. 3(c). A sudden change of slope in the dielectric profile [see inset in Fig. 3(c)] was observed at 318.1 K indicating a transformation in the sample. But no change in the POM textures of the banded spherulites was found at this temperature. We attribute it to the softening of the amorphous component of the sample. On heating, the bands started to become blurred irreversibly at 321.1 K and the texture transformed completely to nonbanded spherulite at 325.1 K. The FESEM studies of this nonbanded spherulite revealed that the lengths of the radially aligned fibrillar crystallites were increased and their distribution was uniform along the radial direction giving rise to the nonbanded texture (see Fig. S5 in the Supplemental Material [56]). Thus the amorphous component after softening gradually transforms to the crystallites and smectic phase on heating which accounts for the observed increase in dielectric constant with increasing temperature before complete melting of the sample to the smectic phase at 327.6 K [41].

Theoretical model

In the last few decades, a few theoretical models based on coherent twisting of fibrils have been introduced to account for banded spherulite. The twisting can occur in a system due to multiple causes such as surface stress mismatch [2,20], isochiral screw dislocation [45,46], autodeformation [8], self-induced concentration or mechanical fields on growth kinetics [47], and topological defects [48]. Some phase field models have also been developed to understand the growth of nonbanded and banded spherulite with twist [49,50]. However, the experimental observations on banded spherulite of 8OCB show no twist in its fibrillar nanocrystallites as discussed earlier. Hence, the above models are not suitable for the description of banded spherulite in this system.

Armed with our experimental results, a time-dependent Ginzburg-Landau (TDGL) model C is developed to account for the rhythmic growth of the banded spherulitic domain observed in our system. This model has been successfully applied in various physical growth phenomena in different systems [51,52]. Kyu *et al.* simulated a ring banded structure using this model and emphasized rhythmic growth assisted banded spherulite formation in polymer blends [53,54]. The model describes the dynamics of a system using a conserved and a nonconserved order parameter. Our experimental studies have clearly established that the growth of alternating concentric crystallite-rich and crystallite-poor zones gives rise to the banded spherulites of 8OCB. Therefore, we define the conserved order parameter $\phi = (\rho - \rho_0)/\rho_0$ which describes the local deviation of density in these zones from the average density ρ_0 of the smectic phase. In addition, the nonconserved order parameter $\psi = (\rho_{nc} - \rho_a)/\rho_0$ describes the local composition, where ρ_{nc}/ρ_0 and ρ_a/ρ_0 are the fractional densities of molecules in the nanocrystalline and amorphous solid phase, respectively. The smectic phase with $\psi = 0$ undergoes a first-order transition to the spherulitic domain with $\psi \neq 0$.

Using these order parameters, the free energy density of the system in its smectic phase can be written as

$$f = \frac{A}{2}\phi^2 + \frac{1}{2}k_\phi|\nabla\phi|^2 + W\left[\frac{\alpha(T)}{2}\psi^2 - \frac{1+\alpha(T)}{3}\psi^3 + \frac{1}{4}\psi^4\right] + \frac{1}{2}k_\psi|\nabla\psi|^2 - \gamma\phi\psi. \quad (1)$$

The first two terms in Eq. (1) represent the free energy associated with the order parameter ϕ of the sample. We assume that ϕ is noncritical across the transition to the spherulitic state and only the terms up to the quadratic order are retained. The third and fourth terms represent the

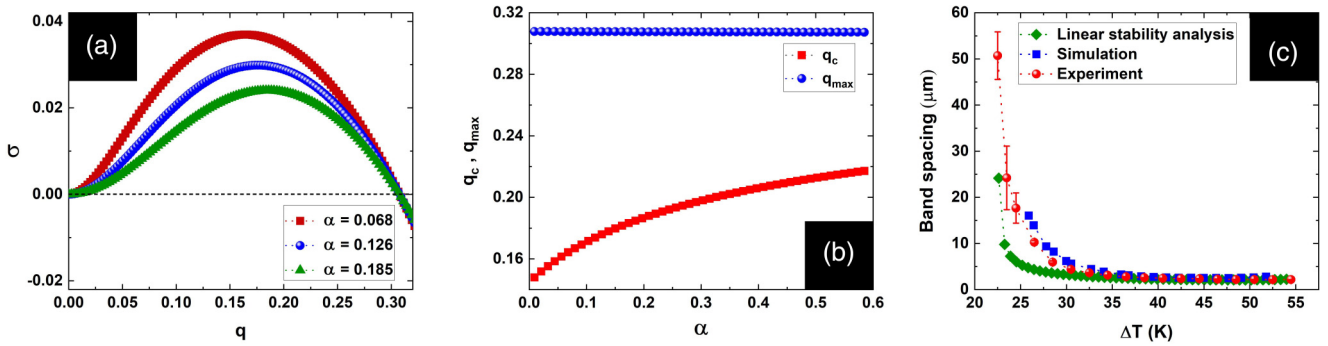

FIG. 4. Effect of supercooling on banded spherulite. (a) The variation of σ with the wave vector q for different values of α. The modes in the wave vector range $0 < q < q_{\max}$ are unstable. (b) The variation of $q_{\max}$ and q_c as a function of α. (c) Comparison between experiment, linear stability analysis, and simulation results for the variation of band spacing with supercooling ΔT. The values of the parameters used for the theoretical model are $\gamma/A = 0.242$, $W/A = 0.1$, $\xi_\phi = 0.04$ μm, $\xi_\psi = 3.16\xi_\phi$, $\lambda_D = 1.41\xi_\phi$.

free energy associated with the order parameter ψ describing the first-order phase transition from the smectic phase to the spherulitic state. Here, $0 \leqslant \alpha(T) = (T - T_c)/(T_m - T_c) \leqslant 1$ is the temperature-dependent parameter driving this first-order transition and T_m, T_c are the melting temperature and supercooling limit of the smectic phase, respectively. The last term in Eq. (1) is the lowest-order coupling between these order parameters.

Using this free energy expansion, the dimensionless form of the TDGL equations for the system can be written as

$$\frac{\partial \phi}{\partial t} = \nabla^2\left[\phi - \frac{\gamma}{A}\psi - \epsilon\nabla^2\phi\right], \tag{2}$$

$$\epsilon\frac{\partial \psi}{\partial t} = -\frac{\xi_\phi^2}{\lambda_D^2}\left[\psi(\psi-1)(\psi-\alpha) - \frac{\gamma}{W}\phi - \epsilon\frac{\xi_\psi^2}{\xi_\phi^2}\nabla^2\psi\right], \tag{3}$$

where $\epsilon = (\frac{\gamma^2}{WA} - \alpha)$ is a dimensionless parameter and $\xi_\phi = \sqrt{\frac{k_\phi}{A}}$, $\xi_\psi = \sqrt{\frac{k_\psi}{W}}$ and $\lambda_D = \sqrt{\frac{A\Gamma_\phi}{\Gamma_\psi W}}$ have the dimension of length. Here Γ_ϕ and Γ_ψ are two dynamical coefficients of the system. The detail derivation of these equations is given in the Supplemental Material [56].

The linear stability analysis (LSA) of Eq. (2) and Eq. (3) was performed to investigate the growth of banded spherulite on quenching the system from the higher-temperature smectic phase. The TDGL equations were linearized with respect to small perturbations $\phi(\vec{r},t) = \delta\phi_0 e^{\sigma t}e^{i\vec{q}\cdot\vec{r}}$, $\psi(\vec{r},t) = \delta\psi_0 e^{\sigma t}e^{i\vec{q}\cdot\vec{r}}$ about the smectic phase ($\phi = 0$, $\psi = 0$). The resulting eigenvalue equations (see Supplemental Material [56]) determine the stability of the smectic phase with respect to these perturbative modes for different values of the control parameter α. The modes with negative real part of σ decay to zero and are therefore stable while the modes with positive real part of σ grow with time and are unstable.

Figure 4(a) shows the variation of σ with the wave vector q for different values of α. As can be seen from Fig. 4(a), σ is positive for modes with wave vector q lying between zero and $q_{\max}$ and these unstable modes give rise to the formation of banded spherulite in this system. Among these unstable modes, σ has the highest positive value for $q = q_c$ and this most unstable mode will be dominant during the growth of the banded spherulite. Figure 4(b) shows the variation of $q_{\max}$ and q_c with the parameter α obtained from LSA. Though q_c varies strongly with α, the $q_{\max}$ does not vary appreciably with it. The wavelength corresponding to this dominant mode calculated from the LSA is compared with the experimentally measured band spacing of the banded spherulite as shown in Fig. 4(c) for different values of supercooling ($\Delta T = T_m - T$). The theoretical result agrees well with the experimental data confirming the general validity of this model.

A general analytical method of finding solutions of the coupled nonlinear TDGL equations given by Eqs. (2) and (3) is not known. These equations were solved numerically under no flux boundary condition using a finite difference method in two dimension. The numerical solutions of the order parameters ϕ and ψ for a banded spherulite growing from a seed at the center are shown in Fig. 5(a) and Fig. 5(b), respectively (also see Fig. S6 in the Supplemental Material [56]). The formation of the ring banded structure is clearly observed as found experimentally. Figure 5(c) shows the graphical profiles of the order parameters along a radial direction of the spherulite. The order parameters vary periodically and in phase along the radial direction during the growth of the spherulite. This in-phase variation of the order parameters arises due to their bilinear coupling with $\gamma > 0$ in Eq. (1).

The physical mechanism of the formation of banded spherulite from the numerical solution of the TDGL model can be understood as follows. In these numerical computations, a banded spherulite grows from an initial nanocrystallite seed on sufficient supercooling of the smectic phase. As the nanocrystallites have higher density compared to the amorphous state, the growth of this nanocrystallite-rich domain leads to decrease in density around it due to the depletion of the molecules arising from the conservation of ϕ. When the density decreases sufficiently, the bilinear coupling between the order parameters ϕ and ψ promotes the formation of a crystallite-poor domain around the previously formed crystallite-rich domain. The growth of this crystallite-poor band in turn increases the density around its periphery and the same bilinear coupling leads to the nucleation of another nanocrystallite-rich band. The growth continues with the formation of alternating crystallite-rich and crystallite-poor bands in a periodic manner along the radial direction of the spherulite as indicated in Fig. 5. The radius of the numerically

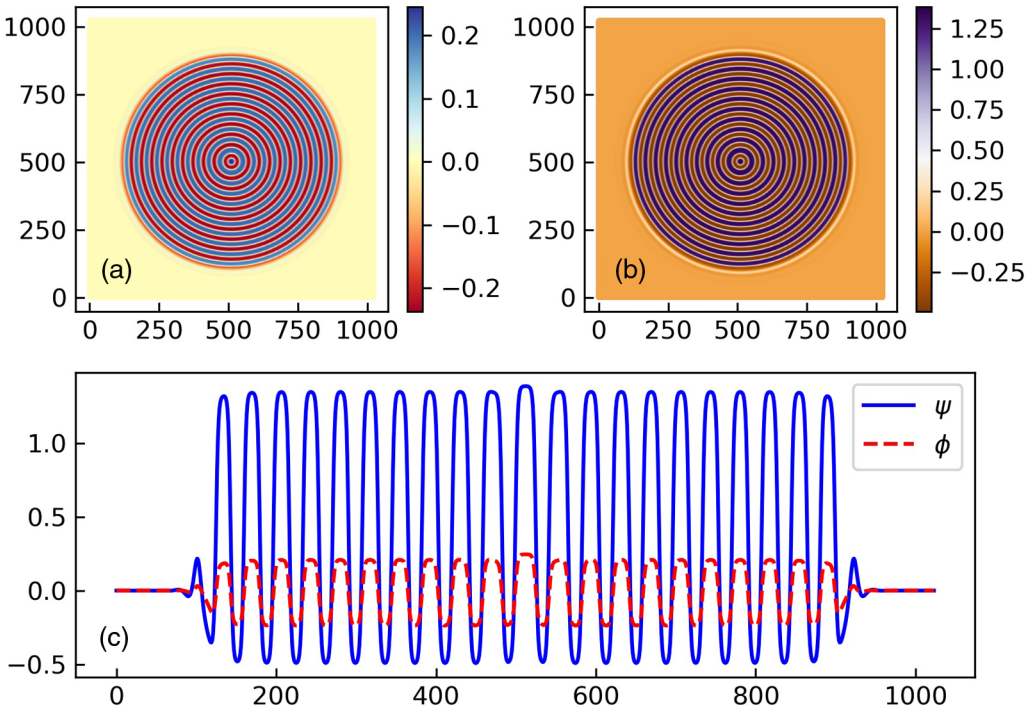

FIG. 5. Simulated banded spherulite domain. The color-coded representation of the order parameters (a) ϕ and (b) ψ of a banded spherulite obtained from the numerical solution of the TDGL equations at $\Delta T = 39.5$ K. The model parameters used are $\gamma/A = 0.242$, $W/A = 0.1$, $\zeta_\phi = 0.04$ μm, $\zeta_\psi = 3.16\zeta_\phi$, $\lambda_D = 1.41\zeta_\phi$, time step size $dt = 0.01$, and spatial step size $dx = dy = 1.0$. (c) The graphical profiles of ϕ and ψ along a radial axis of the simulated banded spherulite.

simulated banded spherulite grows with time in a rhythmic fashion as shown in the Supplemental Material [56], Fig. S7.

The spacing between two successive bands of the spherulite was also calculated from the numerical results for different values of supercooling ΔT. The numerically computed band spacing as a function of supercooling agrees very well with the experimental data as shown in Fig. 4(c). This figure also shows that the experimentally measured band spacing of the spherulite tends to diverge on approaching $\Delta T \sim 22.5$ K from above. Below this supercooling, only the formation of nonbanded spherulites was observed experimentally. Both the LSA and numerical results account for this divergence of band spacing. This divergence arises from a singularity of the TDGL equations for the parameter ϵ in Eqs. (2) and (3) being zero. Therefore, the order parameter ψ is determined by the equation $\psi(\psi-1)(\psi-\alpha) = \frac{\gamma}{W}\phi$ and only the order parameter ϕ controls the dynamics of the system. A comparison between the computed and experimentally measured growth velocities of banded spherulite gives the translational diffusion constant ($A\Gamma_\phi$) of the molecules as 10^{-11} m^2/sec which agrees with the earlier reported data on 8OCB [55]. The consistency of the numerical results was also checked on solving the TDGL equations using the finite element method (FEniCS python package) (see Fig. S8 in the Supplemental Material [56]). However, the numerical solutions of these nonlinear equations show that the ring banded pattern under certain conditions becomes unstable leading to the breaking of the spherical symmetry of the growth pattern. The details on these numerical results will be published elsewhere.

IV. SUMMARY

We have studied the banded spherulitic growth of the solid phase of a pure liquid crystalline compound from its melt. The compound exhibits coexistence of fibrillar nanocrystallites and an amorphous phase in its most stable solid state at room temperature. The banded spherulites are formed due to the rhythmic generation of crystallite-rich and crystallite-poor concentric zones on supercooling the smectic phase of the compound. This produces the modulation in birefringence which gives rise to the interference color bands observed between crossed polarizers. A theoretical model using the time-dependent Ginzburg-Landau theory is developed to account for the observed banded spherulitic growth in this compound which agrees well with the experimental observations.

ACKNOWLEDGMENTS

We thank Vasudha K. N. for her help in acquiring XRD data and K. M. Yatheendran for his help in FESEM and confocal imaging.

[1] B. Crist and J. M. Schultz, Prog. Polym. Sci. **56**, 1 (2016).
[2] B. Lotz and S. Z. Cheng, Polymer **46**, 577 (2005).
[3] G. Lofgren, Am. J. Sci. **274**, 243 (1974).
[4] R. Coish and L. A. Taylor, Earth Planet. Sci. Lett. **42**, 389 (1979).
[5] R. J. Kirkpatrick, Am. J. Sci. **274**, 215 (1974).

[6] I. Minkoff and W. C. Nixon, J. Appl. Phys. **37**, 4848 (1966).
[7] J. Bisault, G. Ryschenkow, and G. Faivre, J. Cryst. Growth **110**, 889 (1991).
[8] A. G. Shtukenberg, Y. O. Punin, E. Gunn, and B. Kahr, Chem. Rev. **112**, 1805 (2012).
[9] R. Beck and J.-P. Andreassen, Cryst. Growth Des. **10**, 2934 (2010).
[10] Y. Oaki and H. Imai, J. Am. Chem. Soc. **126**, 9271 (2004).
[11] A. Thomas, E. Rosseeva, O. Hochrein, W. Carrillo-Cabrera, P. Simon, P. Duchstein, D. Zahn, and R. Kniep, Chem. Eur. J. **18**, 4000 (2012).
[12] C.-Y. Sun, M. A. Marcus, M. J. Frazier, A. J. Giuffre, T. Mass, and P. U. P. A. Gilbert, ACS Nano **11**, 6612 (2017).
[13] U. Al-Atar, A. A. Bokov, D. Marshall, J. M. H. Teichman, B. D. Gates, Z.-G. Ye, and N. R. Branda, Chem. Mater. **22**, 1318 (2010).
[14] P. S. Chow, X. Y. Liu, J. Zhang, and R. B. H. Tan, Appl. Phys. Lett. **81**, 1975 (2002).
[15] J. E. Coleman, B. J. Allan, and B. L. Vallee, Science **131**, 350 (1960).
[16] M. R. H. Krebs, C. E. MacPhee, A. F. Miller, I. E. Dunlop, C. M. Dobson, and A. M. Donald, Proc. Natl. Acad. Sci. U.S.A. **101**, 14420 (2004).
[17] F. Catalina and L. Cifuentes, Science **169**, 183 (1970).
[18] D. Brewster, Trans. R. Soc. Edinburgh **20**, 607 (1853).
[19] H. D. Keith and F. J. Padden, J. Appl. Phys. **34**, 2409 (1963).
[20] H. D. Keith and F. Padden Jr., Polymer **25**, 28 (1984).
[21] A. G. Shtukenberg, J. Freudenthal, and B. Kahr, J. Am. Chem. Soc. **132**, 9341 (2010).
[22] A. G. Shtukenberg, X. Cui, J. Freudenthal, E. Gunn, E. Camp, and B. Kahr, J. Am. Chem. Soc. **134**, 6354 (2012).
[23] W. Pisula, M. Kastler, D. Wasserfallen, T. Pakula, and K. Müllen, J. Am. Chem. Soc. **126**, 8074 (2004).
[24] X. Cui, A. L. Rohl, A. Shtukenberg, and B. Kahr, J. Am. Chem. Soc. **135**, 3395 (2013).
[25] A. Shtukenberg, J. Freundenthal, E. Gunn, L. Yu, and B. Kahr, Cryst. Growth Des. **11**, 4458 (2011).
[26] T.-F. Lin, R.-M. Ho, C.-H. Sung, and C.-S. Hsu, Chem. Mater. **18**, 5510 (2006).
[27] J. L. Hutter and J. Bechhoefer, Phys. Rev. Lett. **79**, 4022 (1997).
[28] J. L. Hutter and J. Bechhoefer, J. Cryst. Growth **217**, 332 (2000).
[29] C. Wang, R. Thomann, J. Kressler, Y. Thomann, K. Crämer, B. Stühn, P. Svoboda, and T. Inoue, Acta Polymerica **48**, 354 (1997).
[30] J. Chen and D. Yang, Macromolecules **38**, 3371 (2005).
[31] J. Chen and D. Yang, J. Polym. Sci., Part B: Polym. Phys. **45**, 3011 (2007).
[32] Y. Okabe and T. Kyu, Polymer **45**, 8485 (2004).
[33] H. Uesaka and R. Kobayashi, J. Cryst. Growth **237-239**, 132 (2002).
[34] Y. Li, H. Huang, T. He, and Z. Wang, Polymer **54**, 6628 (2013).
[35] Y. Yamazaki, M. Kikuchi, A. Toda, J.-i. Wakita, and M. Matsushita, J. Phys. Soc. Jpn. **83**, 064002 (2014).
[36] Y. Li, H. Huang, Z. Wang, and T. He, Macromolecules **47**, 1783 (2014).
[37] Y. Li, Z. Wang, Q. Gu, and X. Wu, RSC Adv. **6**, 45241 (2016).
[38] Y. Li, Z. Wang, and T. He, Crystals **7**, 115 (2017).
[39] J. Wei, L. Wu, H. Zhu, Y. Li, and Z. Wang, CrystEngComm **22**, 7016 (2020).
[40] B. Fang, J. Wei, S. Qiu, J. Zhu, L. Wu, and Y. Li, J. Cryst. Growth **575**, 126372 (2021).
[41] S. Ghosh and A. Roy, RSC Adv. **11**, 4958 (2021).
[42] A. Shtukenberg, E. Gunn, M. Gazzano, J. Freudenthal, E. Camp, R. Sours, E. Rosseeva, and B. Kahr, ChemPhysChem **12**, 1558 (2011).
[43] E. M. Woo, G. Lugito, and C.-E. Yang, CrystEngComm **18**, 977 (2016).
[44] K. Hori, M. Kuribayashi, and M. Iimuro, Phys. Chem. Chem. Phys. **2**, 2863 (2000).
[45] D. Patel and D. Bassett, Polymer **43**, 3795 (2002).
[46] A. Toda, T. Arita, and M. Hikosaka, Polymer **42**, 2223 (2001).
[47] J. M. Schultz, Polymer **44**, 433 (2003).
[48] Y. Hatwalne and M. Muthukumar, Phys. Rev. Lett. **105**, 107801 (2010).
[49] L. Gránásy, T. Pusztai, G. Tegze, J. A. Warren, and J. F. Douglas, Phys. Rev. E **72**, 011605 (2005).
[50] A. Fang and M. Haataja, Phys. Rev. E **92**, 042404 (2015).
[51] A. A. Wheeler, W. J. Boettinger, and G. B. McFadden, Phys. Rev. A **45**, 7424 (1992).
[52] K. R. Elder, F. Drolet, J. M. Kosterlitz, and M. Grant, Phys. Rev. Lett. **72**, 677 (1994).
[53] T. Kyu, H.-W. Chiu, A. J. Guenthner, Y. Okabe, H. Saito, and T. Inoue, Phys. Rev. Lett. **83**, 2749 (1999).
[54] H. Xu, H.-W. Chiu, Y. Okabe, and T. Kyu, Phys. Rev. E **74**, 011801 (2006).
[55] S. V. Dvinskikh and I. Furó, Phys. Rev. E **86**, 031704 (2012).
[56] See Supplemental Material at http://link.aps.org/supplemental/10.1103/PhysRevMaterials.6.053401 for detailed theoretical model, linear stability analysis, variation of band spacing with sample thickness, SEM textures, Raman peak for CN stretching mode, rhythmic variation of banded spherulite radius, and other simulation results.